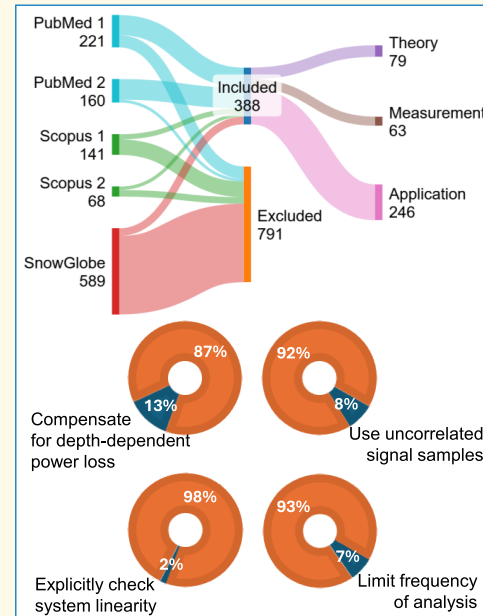


# A Systematized Review of Quantitative Ultrasound Based on First-Order Speckle Statistics

Alexandra M. Christensen<sup>ID</sup>, Ivan M. Rosado-Mendez<sup>ID</sup>, Member, IEEE,  
and Timothy J. Hall<sup>ID</sup>, Life Member, IEEE

**Abstract**—Since the late 1970s, the speckle interference patterns ubiquitous in pulse-echo ultrasound images have been used to characterize subresolution tissue structures. During this time, new models, estimation methods, and processing techniques have proliferated, offering a wealth of recommendations for the task of tissue characterization. A literature review was performed to draw attention to these various methods and to critically track assumptions and gaps in knowledge. A total of 388 articles were collected from a systematic search for first-order speckle statistics in diagnostic ultrasound in the NIH PubMed database and Elsevier's Scopus database. Articles were grouped by basic characteristics and evaluated for addressing fundamental assumptions. A sampling of models and methods is presented to reveal the state of the art in speckle statistics as well as sources of measurement error and other important considerations. While this body of literature emphasizes the value of speckle analysis in diagnostic ultrasound, it is shown that relatively little attention is devoted to basic assumptions such as the linearity of system response and scatterer geometry. Additionally, several areas of investigation are available to improve upon speckle statistics analysis, potentially leading to the advancement of this unique tool.



**Index Terms**—Envelope statistics, homodyned K, Nakagami, parameter estimation, quantitative ultrasound, Rayleigh, speckle statistics, systematic literature review, tissue characterization.

## I. INTRODUCTION

SPCKLE statistics analysis is a method of quantifying the interference patterns formed when coherent imaging systems encounter subresolution heterogeneity. Without direct observation of these microscopic components, statistical

Manuscript received 22 April 2024; accepted 14 May 2024. Date of publication 17 May 2024; date of current version 15 July 2024. This work was supported by the Eunice Kennedy Shriver National Institute of Child Health and Human Development under Award R01HD096361 and Award R01HD072077. The content is solely the responsibility of the authors and does not necessarily represent the official views of the National Institutes of Health. (*Corresponding author:* Alexandra M. Christensen.)

Alexandra M. Christensen and Timothy J. Hall are with the Department of Medical Physics, University of Wisconsin–Madison, Madison, WI 53705 USA (e-mail: amchristens4@wisc.edu; tjhall@wisc.edu).

Ivan M. Rosado-Mendez is with the Departments of Medical Physics and Radiology, University of Wisconsin–Madison, Madison, WI 53705 USA (e-mail: rosadomendez@wisc.edu).

This article has supplementary downloadable material available at <https://doi.org/10.1109/TUFFC.2024.3402560>, provided by the authors. Digital Object Identifier 10.1109/TUFFC.2024.3402560

models are derived to describe the macroscopic texture in the envelope of an ultrasonic signal. As a result, valuable information can be obtained through analyzing speckle patterns which would not be easily extracted in qualitative ultrasound imaging [1], [2], [3].

Certain assumptions must be met to correctly interpret statistical parameters that describe speckle, and models must be appropriate for describing the underlying microstructure. In any tissue characterization task, it is important to thoroughly understand the methods and models previously studied to make accurate and precise measurements. The purpose of this literature review is to: 1) draw attention to the numerous models and parameter estimation methods that exist to describe ultrasound speckle from theoretical acoustic interactions in media and 2) note factors in data acquisition and parameter estimation that may affect speckle statistical analysis, outlining choices that must be made by the researcher using this tool.

Models for describing speckle differ, but the underlying paradigm of speckle formation is generally consistent:

### Highlights

- This review provides a critical overview of models and methods in first-order speckle statistics for quantitative ultrasound.
- Many advances in speckle statistics analysis have been made, but opportunities for improvement exist in explicitly addressing model assumptions and systematically analyzing measurement errors.
- As commercial implementation of speckle statistics continues, along with the demand for quantitative biomarkers, careful tracking of assumptions and sources of estimation error is crucial.

the structures that cause speckle interference patterns are modeled as discrete “scatterers,” or variations in density and compressibility from the background medium [4]. Assuming weak scattering, that is, a single scattering paradigm [3], each scatterer that encounters an acoustic wave will produce an echo with an amplitude and phase component. Each echo’s complex amplitude depends on the magnitude and angular distribution of scattered pressure [2], and its phase depends on the distance from the acoustic source to the signal receiver.

The total echo formed by the interference of the waves scattered by a number of discrete scatterers is represented as a “random walk” or superposition in the complex plane within one resolution unit, where the resulting echo amplitude is given by the sum of the individual phasors [5], [6]. The resolution cell is the finite region in space that contributes to a single signal sample, often defined as the region where the received signal is  $-6$  dB or greater compared to the peak value for a point scatterer placed within it [2]. This means that scatterers are only measured in aggregate, that is, the size and location of scatterers are not directly measured; therefore, resulting signals are modeled as statistical quantities giving rise to an overall expected probability distribution for the amplitudes of the echo envelope. When scatterers are uniformly positioned in space, phase is uniformly distributed between  $0$  and  $2\pi$ ; otherwise, there is deviation from the uniform distribution [7], [8], [9]. It is generally assumed that a scatterer’s size and position are independent quantities and that scatterer properties are independent of other scatterers [3], [5]. Working from these basic principles, Burckhardt [6] applied the Rayleigh distribution to describe speckle statistics from diffuse scatterers in 1978. Wagner et al. [1] made use of the more general Rician distribution for structured scattering in 1983, and Weng et al. [10] applied the K distribution to describe clustered scatterers in 1991. These scenarios have been termed “Post-Rayleigh” and “Pre-Rayleigh,” respectively. In 1994, Dutt and Greenleaf [11] used the homodyned K distribution to generalize all three models, and, in 2000, Shankar [12] demonstrated that the Nakagami distribution is a suitable approximation to the homodyned K. These models form the basis for the vast majority of first-order speckle statistics analysis in quantitative ultrasound. Fig. 1 summarizes these statistical regimes and the scatterers that produce them. Fig. 2 provides a general description of how speckle statistics are typically estimated from data acquired by ultrasound.

Every model used to describe the statistics of speckle involves a set of assumptions about the data acquired by diagnostic ultrasound. Some common assumptions include sample independence (i.e., independent, identically distributed

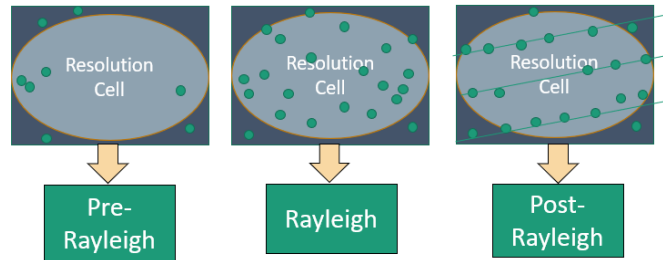


**Fig. 1.** Three main scenarios discernable with first-order speckle statistics are the pre-Rayleigh caused by sparse or clustered scatterers, Rayleigh caused by diffuse scatterers, and post-Rayleigh caused by aligned or periodically arranged scatterers. These scenarios exist within the context of the resolution unit of the acoustic beam, that is, the resolution cell. The resolution unit, here depicted as an ellipse, is defined as the region in space that contributes to a single received signal sample.

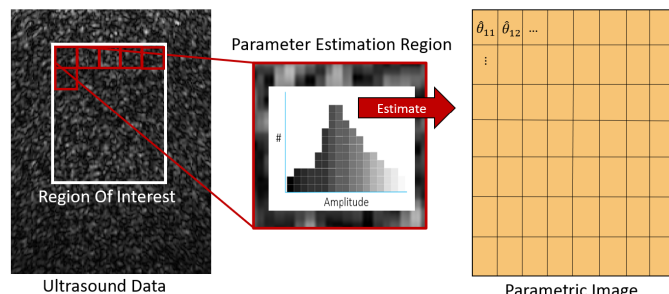


**Fig. 2.** Envelope statistics analysis in diagnostic ultrasound begins with defining an ROI in which speckle statistics estimates,  $\hat{\theta}$ , will be calculated. The ROI may further be subdivided into smaller PERs in which the histogram of signal amplitudes will be characterized. In many cases, PERs are allowed to overlap to improve parametric image resolution. An image of speckle estimates may be formed from the parameters calculated in each PER,  $\hat{\theta}_{i,j}$ .

(i.i.d.) samples of the echo signal), independence of scatterers’ amplitude and location, validity of the Born approximation, isotropic scattering, linear response of the ultrasound system, and homogeneity of the medium [3], [5]. These assumptions can be limiting, especially when considering the complexity of biological tissues in practical applications. Additionally, speckle statistics is system-dependent, relying on the properties of the acoustic pulse which determines resolution. These properties must be known to characterize the medium since the echo envelope depends on both the medium and the system. Noise, whether electronic/thermal or from nonspeckle signals such as large reflectors or imaging artifacts, can affect speckle statistics, as these create distortions in amplitude unrelated to the interactions described by speckle models. Likewise, attenuation and diffraction effects are not accounted for and will affect speckle statistics. Assumptions about scat-

terers themselves may also not hold true. For example, point scatterers may be a poor description of biological structures, or multiple scattering may contribute significantly to a received signal.

Bearing this complexity in mind, it is important to carefully consider the available options and assumptions involved at each step of the process for using speckle statistics in tissue characterization. Appropriate models for the tissue of interest must be chosen, and data should be acquired while considering possible confounding factors and sources of noise. Parameter estimation methods must balance bias, variance, and practical considerations such as computation efficiency. Parametric maps are created by subdividing the region of interest (ROI) into smaller parameter estimation regions (PERs) and can reveal localized differences in tissue structure; here, the tradeoff between estimate stability and resolution must be considered. To make informed decisions in speckle statistics, a careful and critical search of the available literature is needed. This is especially relevant as commercial implementations of first-order speckle statistics are emerging in clinical ultrasound systems, such as acoustic structure quantification (ASQ; Canon Medical Systems) [13] and tissue scatter-distribution imaging (TSI; Samsung Medison) [14].

This review is intended to provide a representative overview of state-of-the-art methods in first-order speckle statistics for quantitative ultrasound. The search for relevant articles was performed under recommendation for a “systematized” review [15], namely in that inclusion and exclusion criteria were defined before the search, a careful record of queries and results was kept throughout the search, and a broadly comprehensive literature body was sought. Section II elaborates on the search methods, and Section III contains the results. Section III is further broken into the significant models, sources of measurement error, and parametric imaging considerations contained within the search.

## II. METHODS

Articles were found using the National Institute of Health PubMed database and Elsevier’s Scopus database in February 2024. The exact queries are provided in the Supplementary Material. The title and abstract of all results were scanned for inclusion based on relevance to first-order speckle statistics in diagnostic ultrasound. Preprint articles and conference proceedings were excluded, whereas book chapters and published peer-reviewed journal articles and reviews were included. Papers primarily concerned with second-order statistics or texture analysis, nonmedical ultrasound, and applications relating to speckle tracking or speckle reduction were excluded. Only articles available in English were reviewed. After the initial search, additional articles were found by searching for terminology that emerged during the first search; the five most common models specifically were sought. The titles and abstracts of these secondary findings were scanned and either included or excluded using the same criteria as above. Because PubMed was explored first in both the primary and secondary searches, many Scopus results were excluded due to repetition; this partially contributes to the lower inclusion rate of Scopus findings.

To further ensure comprehensiveness, works cited in the included literature body and works that cited the included

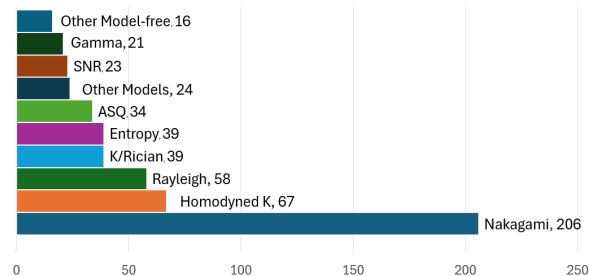


**Fig. 3.** Number of articles employing each main speckle statistics model. The sum is greater than the total number of articles found because many publications employ more than one model.

literature body were searched using SnowGlobe [16], an iterative search tool designed for systematic literature review. Only results with five or more connections (i.e., forward or backward citations) within the included database results were considered, since works with fewer connections are less likely to be relevant to this review. SnowGlobe results were then subject to the same inclusion and exclusion criteria as above.

Included articles were grouped by basic characteristics, such as year published, tissue application, and models used. Additionally, each included article was manually searched to evaluate whether the assumptions of system linearity, sample independence, narrowband signal reception, and absence of attenuation and diffraction were addressed, if applicable to the experiments detailed.

## III. RESULTS

A total of 1179 search results were viewed from the database and Snowball search, of which 388 were included after evaluating for inclusion criteria and removing duplicates. Of the included articles, 278 were found by the PubMed database searches, and 58 were found on Scopus but not Pubmed. The SnowGlobe search found 589 articles with five or more connections; however, after removing duplicates and evaluating inclusion criteria, only 52 were included. The majority of articles primarily reported measurements in specific disease applications, leaving 142 detailing novel models, parameter estimation methods, and interpretation insights in speckle statistics for biomedical ultrasound. Breakdowns of these totals by contribution type, primary model, tissue application, and year of publication are given in Figs. 3–5. These breakdowns provide insights into the focuses of research in speckle statistics; for example, the main tissues of interest are liver, breast, and cardiovascular applications. While the Nakagami and homodyned K distributions are the most commonly used in speckle analysis, almost one-third of found literature uses other models. A full list of articles found in the database searches and SnowGlobe can be found in the Supplementary Material.

Out of all articles where it may be relevant (e.g., excluding theory-only manuscripts), only 8% were found to aim toward using i.i.d. samples in their parameter estimation. Additionally, 7% of articles mentioned limiting the bandwidth of analysis, and 13% compensate for power loss due to attenuation or diffraction. Even more rare, 2% of articles using physical ultrasound systems were found to explicitly check for system response linearity.

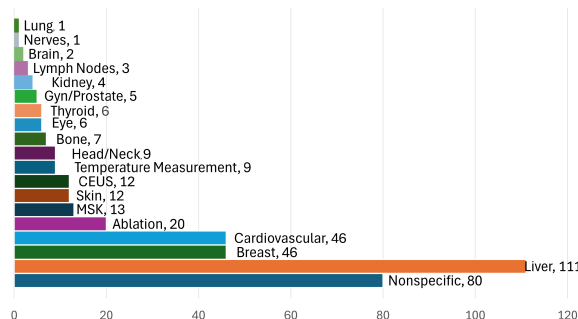


**Fig. 4.** Number of articles focused on each tissue application. The sum is greater than the total number of articles found because many publications apply analysis to more than one tissue.

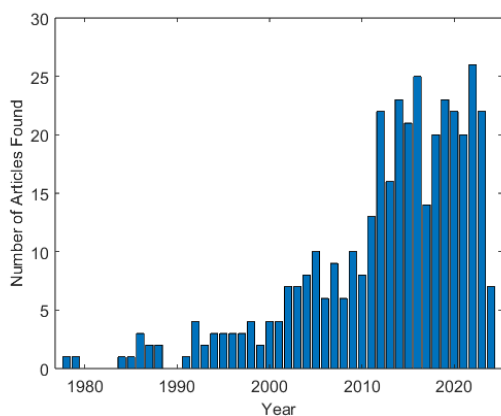


**Fig. 5.** Number of articles included in the search by year of publication.

#### A. Models for First-Order Speckle Statistics

As summarized in Fig. 3, the most prominent models in the literature are the Nakagami and homodyned K. However, much of the literature is dedicated to others, some of which have not gained much traction outside of their original introduction. The purpose of this section is to show the motivation and meaning behind using the “state-of-the-art” Nakagami and homodyned K distributions but also to draw attention to models (and model-free features) that deviate from these norms and to highlight their potential benefits.

**1) Nakagami and Homodyned K:** The Nakagami and homodyned K distributions are both used as general models for ultrasonic speckle, able to differentiate between Rayleigh, pre-Rayleigh, and post-Rayleigh conditions. The Nakagami is the most commonly used, due to ease of calculation [3]. However, an advantage of the homodyned K distribution is that the parameters have physical meaning since the model is derived from scattering physics, whereas the Nakagami distribution is an approximation of the enveloped histogram [17]. The  $\alpha$  parameter of the homodyned K distribution describes the degree of scatterer clustering in media, and the  $k$  parameter represents the ratio of coherent to diffuse scattering,  $k = (\epsilon/\sigma)$  [11] (alternatively defined as  $k = (\epsilon/\sigma\sqrt{\alpha})$  [18]). Conversely, only one parameter of the Nakagami distribution,  $m$ , can differentiate scatterer conditions, and there is ambiguity between scatterer density and the presence of coherent scattering [12]. The  $\Omega$  parameter of the Nakagami distribution is related to signal power and is, therefore, not typically useful in tissue characterization since it depends on

operator settings like transmit power and gain. Additionally, the emergence of machine learning homodyned K parameter estimation [19] suggests that computational advantages of the Nakagami distribution are perhaps overemphasized.

Relating the parameters of the homodyned K distribution to the physical properties of scatterers is of particular interest. Destrempe et al. [20] derived a relationship between the coherent and diffuse signal powers and the backscatter coefficient, a spectral parameter which, under the spherical Gaussian model, relates to effective scatterer size and acoustic concentration. By relating these parameters, they were also able to derive a relationship between envelope statistics and a packing factor in the case of concentrated media such as aggregated blood cells. Hu et al. [21] provide an assessment of the physical meaning of homodyned K parameters relating to a variety of spatial distributions of scatterers. Fernandez et al. [22] derived a third-degree polynomial relating  $\alpha$  to the concentration of suspended scatterers. The authors note, however, that the relationship they derived depends on the ultrasound system and the presence of Rayleigh scattering; a universal relationship could not be derived.

Currently, the most common estimator due to low bias and variance is the method proposed by Destrempe et al. [18]. This method uses the first moment of measured intensity and the U- and X-statistics previously introduced in K-distribution estimation and is thus called the “XU” method. These statistics are set equal to analytic counterparts derived from the homodyned K distribution. The XU method is generally considered to outperform previously derived methods using even amplitude moments [11] or the signal-to-noise ratio (SNR), skewness, and kurtosis of signal samples [23], [24]. However, this method requires several thousand samples to avoid standard deviation on par with estimates themselves [25]. This presents problems when imaging small anatomy or heterogeneous tissue regions. Large sample sizes are not as crucial for parameter estimation with the Nakagami distribution which might make it a more appropriate model in some cases than the homodyned K [26].

Computation time is another challenge for the practicality of homodyned K estimators. Neural networks have been used to mitigate this problem. Zhou et al. [19] proposed an artificial neural network (ANN) with inputs of SNR, skewness, kurtosis, X-statistic, and U-statistic, with outputs of  $\alpha$  and  $k$  parameters of the homodyned K distribution. The neural network had lower mean normalized standard deviation and mean relative root mean squared error (RMSE) than the XU method, while the XU method performed better in terms of mean relative bias between estimates and target values. Importantly, however, the neural network improved computation time by an order of magnitude. Later, Gao et al. [27] modified the neural network using the optimal orders of skewness, kurtosis, and SNR for homodyned K estimation found by Hruska and Oelze [24], namely 0.72 and 0.88. This neural network outperformed the original. A maximum likelihood estimator proposed by Liu et al. [28] was able to achieve higher accuracy with a lower sample size than Zhou et al.’s neural network method or the XU method; however, its computational costs are higher than that of XU. Liu et al. later proposed a table search algorithm that was more accurate and faster than XU or ANN [29].

Tehrani et al. [30] compared mean absolute error and relative root mean squared error of several estimation methods of homodyned K parameters, including the XU method, Liu's table search method, and their own Bayesian neural network (BNN), each with or without an autoencoder neural network for denoising inputs to each estimator. It was observed that the autoencoder provides improvements in all estimators, although less substantially in the BNN due to its learning of noise features. Similar to the neural network of Zhou et al., the BNN reduced computation time by more than an order of magnitude compared to the XU method. It was also observed that each estimation method has ranges of  $\alpha$  and  $k$  in which it performs best, so the optimal estimator may be task-dependent.

For the Nakagami distribution, moments-based methods are the simplest ways to estimate the  $m$  parameter. The method-of-moments estimator of  $m$  is the SNR of envelope intensity, that is, the amplitude squared. While moments-based methods are simple and produce low bias, lower variance may be obtained by using maximum-likelihood estimation (MLE) [3], [31]. Due to its transcendental form, the MLE can be solved by approximation as in the Tolyparev–Polyakov, Lorenz, or Greenwood–Durand estimators, or by the recursive Bowman method [32]. Kolar et al. [32] demonstrated that the Greenwood–Durand and Bowman estimators equally provided the lowest  $\chi^2$  error in  $m$ , and Wang et al. [33] similarly demonstrated that these estimators provided lower RMSE compared to those previously mentioned. Other iterative methods such as binary search or Newton–Raphson have also been used to solve for  $m$  in the maximum likelihood formulation [3], [25].

**2) Model Modifications:** Where the Rayleigh, Rician, K, and later Nakagami and homodyned K distributions may be inadequate to describe tissue, researchers have derived modifications to address certain complexities. For example, there has been interest in statistical quantities related to the Rayleigh distribution [34]. Yamaguchi and Hachiya [35] and Yamaguchi et al. [36] used a constant false alarm rate (CFAR) technique to enhance non-Rayleigh features in cirrhotic liver. Yamaguchi et al. [37] also used Q–Q plots to assess the deviation of envelope statistics from the Rayleigh distribution. Based on CFAR, Yamaguchi et al. [38] further proposed a fiber structure extraction technique (FSET) to identify non-Rayleigh components and quantify liver fibrosis. Toyoda et al. [39] introduced a method for plotting the histogram of a modified chi-squared value between the Rayleigh distribution and acquired data. This method was later referred to as ASQ as it became commercially implemented [34], [40], [41].

The Nakagami distribution has also been modified for improved modeling. Concerned with the inadequacy of the Nakagami distribution to match the tails of acquired data, Shankar [42] introduced a correction factor to account for this error. The reason given for focusing on the tails is that they are crucial in minimizing Type I and Type II classification errors and thus may be critical for reliable tissue classification. The new “generalized” Nakagami model is expressed with a correction factor parameter. The generalized Nakagami model more closely represented tissue-mimicking phantom data than the Nakagami, and it was more sensitive to scatterer density.

Shankar [43] later adjusted the Nakagami model to account for scenarios in which  $\Omega$  could itself be a gamma-distributed

random variable, such as in highly nonstationary signals. Agrawal and Karmeshu [44] also noted the limited ability of the Nakagami distribution to fit the tails of acquired echo data, as well as the random variance in backscattered power due to multiple scattering or shadowing. The authors modeled these random fluctuations by a lognormal distribution, using an inverse Gaussian distribution as an approximation of the lognormal distribution. This results in a closed-form Nakagami Inverse Gaussian distribution. Agrawal and Karmeshu [45] further explored this idea by applying the generalized inverse Gaussian distribution to the Nakagami probability function, forming the Nakagami-generalized inverse Gaussian distribution. In a similar vein, Nadarajah [46] proposed 13 models and their estimators based on the Nakagami distribution compounded with other distribution families; however, these were not applied to any ultrasound imaging or simulation data.

While modifications of the Nakagami distribution typically demonstrate better fitting to ultrasonic data, Destrempe and Cloutier [17] note that only the homodyned K distribution offers a limiting infinite SNR corresponding to vanishing inhomogeneity in the medium. This is another way in which the homodyned K model contains more physical meaning than the Nakagami family.

**3) Multimodels:** All of the above models assume that the medium contains scatterers that produce echoes with a single distribution of amplitudes and phases, that is, one type of scattering. Since tissues may contain multiple types of scatterers with different properties, several authors have proposed weighted sums of traditional models as better descriptors.

Igarashi et al. [47] proposed a weighted summation of two Rayleigh distributions to quantify the amount of cirrhotic tissue present in the liver. This model was shown to have better agreement with clinical data than a single Rayleigh distribution. Higuchi et al. [48] later extended this mixture to three Rayleigh distributions. Seabra et al. [49] used an arbitrary number of Rayleigh distributions, modeling tissue as a weighted sum of Rayleigh distributions called the Rayleigh Mixture Model. The Rayleigh Mixture Model outperformed a single Rayleigh distribution in Kullbeck–Liebler divergences for three types of arterial plaque, showing that this more complex model is better suited to such clinical applications. These models require either the number of distributions to be known beforehand or for multiple numbers of terms to be tried and compared. Mori et al. [50] later proposed a method for estimating the number of tissue components present in an envelope sample using empirical thresholds of signal moments. Optimal moment inputs were later chosen [51].

Tamura et al. [52] proposed a double Nakagami distribution in the form of a weighted sum of Nakagami distributions with different parameter values. Estimates were made for the Nakagami value of fatty liver tissue and the values of two weights which sum to unity, and the Nakagami value for the background tissue was treated as a known value from the previous measurement. They showed that the double Nakagami model had lower Kullbeck–Liebler divergence than the single Nakagami model in numerical simulations with varying degrees of secondary scatterers.

Destrempe et al. [20] proposed a mixture of homodyned K models to address varying statistics within an ROI. The

authors used a segmentation algorithm based on a Markov Random Field model to divide the ROI into a finite number of subregions. Parameter estimation then only included pixels within the same subregion.

**4) Other Statistical Models:** While the Rayleigh, Rician, K, homodyned K, and Nakagami distributions are cited often in characterizing ultrasound speckle, other models have been developed for various specific applications. Although less widely used, these distributions should not be ignored, as insights into these models could be useful beyond the tissue or disease for which they were originally derived.

The gamma distribution has been applied to log-compressed envelopes in B-mode images [53]. To account for structural heterogeneity, the gamma distribution is sometimes applied in weighted sums [43], [54], [55], [56], [57]. The gamma distribution is related to the Nakagami, as the cumulative distribution function of the Nakagami distribution is a gamma distribution [12], and since the square (intensity in diagnostic ultrasound) of Nakagami-distributed samples are necessarily gamma-distributed [54], [58]. To estimate the parameters of a mixture of gamma distributions, Destrempe et al. [54] designed an estimation maximization algorithm for computing a maximum a priori estimate.

The gamma distribution (and the Nakagami) is a special case of the more complex generalized gamma distribution. Similar to the generalized Nakagami distribution, the generalized gamma can account for the heavier tails of speckle distributions and is also presented in a mixture form [59].

Shankar [60] introduced the McKay probability density function to model speckle resulting from microcalcifications. The McKay model can also be generalized to all other cases contained in the Nakagami model. It was shown that this model results from a sum of correlated gamma-distributed variables. The McKay, gamma, and gamma mixture models were compared in the case that a boundary between regions of different scatterer densities exists within the PER [58]. Both the gamma mixture and the McKay models provided better fits to measured envelope distributions.

Parker [61] developed a model to describe speckle resulting from cylindrical scatterers arranged in isotropic fractals, which is a deviation from the canonical model of spherical scatterers with Gaussian form factors. These cylindrical scatterers may provide a more accurate description of tissues like the liver, which is composed of branching vasculature. In this scenario, the ultrasound pulse is assumed to interact with a single cylindrical scatterer with a radius given by a power law probability distribution related to the tissue's fractal dimension. The resulting amplitude distribution is the Burr type XII distribution, which more closely fit histograms of rat and human liver tissue than the Rayleigh distribution. Adding to their analysis, Parker and Poul [62] derived probability distributions for signal intensity and log-compressed envelopes from the same set of assumptions, and arrived at the Lomax distribution and generalized logistic distribution, respectively. This analysis agrees with that of Lowerison et al. [63] who used the Lomax distribution earlier in quantifying signals from angiogenic tumors. Parker and Poul also examined a complex summation of Burr distributed amplitudes for the case in which

there is more than one cylindrical scatterer per resolution cell and analytically showed that an increase in the power law dependence on fractal dimension is expected, which is consistent with their previous result.

**5) Model-Free Features:** In addition to calculating estimators of theoretical probability density functions, speckle may also be characterized by making direct calculations from acquired data. These features are described as model-free, as opposed to the model-based parameters that come from distribution estimates. Model-free features have the advantage of not requiring that samples follow a specific distribution.

SNR is a widely used model-free feature. As the scatterer configuration diverges from fully developed diffuse scattering, the SNR of echo signal amplitude also changes, diverging from the Rayleigh-distributed value of 1.91 [64], [65]. The SNR may be calculated from amplitude as stated, or from higher or fractional order moments of the signal. The fractional-order SNR has the advantage of lower bias and variance and also requires fewer samples for estimation [66].

The kurtosis of a signal envelope is the normalized fourth central moment which is thought of as a quantifier of the peakedness of the signal histogram [67]. Kurtosis was proposed by Kuc [67] in 1986 as an indicator of liver steatosis, since signal envelopes from the healthy and diseased liver were observed to produce different peak features. Kurtosis can be used to measure the deviation of a process from a Gaussian distribution, in which it approaches a value of 3. Kurtosis is often used alongside other statistical quantities or as a step in parameter estimation; however, kurtosis images have also been proposed for the detection of fatty liver [68].

Hughes [69] proposed the use of entropy in ultrasonic imaging for characterizing microstructure. Entropy can be considered a measure of the homogeneity of a region, related to the local variance [70]. In other words, it is a measure of information contained in each amplitude measurement of an ultrasound echo signal. Entropy is also robust to non-linear transformations such as log compression, which is an advantage when raw data is not readily available [71]. Zimmer et al. [70] demonstrated the use of local Shannon entropy for region segmentation of ovarian cysts since histograms of fluids have less gray-level spread than soft tissues. Several authors have found entropy imaging with small estimation region sizes more effective than Nakagami imaging in ROC curves for detection tasks [72], [73], [74]. The reason may be due to complex structures in the tissue background that cause the amplitude distribution to deviate farther away from the Nakagami distribution than expected at small sample sizes [74]. Smolikova et al. [75] proposed to use the low-order Renyi or Tsallis entropies for ultrasound tissue characterization, since they have higher dynamic range with respect to scatterer density and spacing compared to Shannon entropy. Chan et al. [76] compared Shannon entropy to sample entropy and found evidence of improved clinical performance in clinical liver steatosis and fibrosis characterization tasks using the latter. Sorriento et al. [77] used sample entropy of signal phase to characterize bone tissue.

Rising interest in entropy and entropy imaging has inspired improved estimation methods. Estimation of Shannon entropy

is often histogram-based [70], [73], which introduces the question of ideal bin scheme. One way of mitigating this dependence is a normalization scheme [78] which limits bins to between 0 and 1, improving contrast and detection ability. Gao et al. [79] instead proposed a kernel density estimator based on a Gaussian kernel for probability density function estimation, resulting in similar clinical performance to histogram methods but greater dynamic range. Li et al. [80] proposed a  $k$  nearest neighbor method with success in improving contrast-to-noise ratio and classification accuracy in clinical applications compared with histogram methods.

**6) Phase Statistics:** The probability distributions covered thus far describe the statistics of envelope amplitude or intensity. However, important information is also contained in the signal phase. Weng et al. [7] demonstrated that in 1-D ultrasound simulations of regularly spaced scatterers, phase distributions showed clear “bias” from uniformity when scatterers were spaced by quarter wavelengths and slight bias when spaced by half wavelengths. However, this bias disappeared if spacing variance was increased to 50%, suggesting that scatterer spacing must be somewhat consistent to be evident in signal phase statistics. Weng et al. [8] additionally proposed a technique in which to detect regularly spaced scatterers. This was done by demodulating the received signal by a range of frequencies and then computing metrics of phase nonuniformity as a function of frequency. These metrics were shown to peak at the demodulation frequency whose quarter wavelength corresponds to scatterer spacing. Narayanan et al. [9] extended the analysis to quasi-periodic scatterers. Metrics of phase uniformity included a  $\chi^2$  test and the measured SNR of phase. Shankar et al. [81] used a  $\chi^2$  test to show that phase statistics deviate significantly from uniformity for periodic and quasiperiodic scattering. Shankar [12] also used the  $\chi^2$  test to reduce the ambiguity in Nakagami analysis between scattering density and coherence caused by periodic scatterer spacing.

**7) Model Simplifications:** The foundational derivation (see Section I) of speckle models is relatively simple, accounting only for a set of  $N$  point scatterers within a resolution cell. Each resolution cell produces an amplitude sample that follows a probability distribution. Therefore, anything that affects received amplitudes and their probability distribution other than the number and spatial distribution of scatterers can alter speckle statistics estimates and should be understood in the interpretation of resulting parameters.

In deriving most speckle statistics models, it is assumed that the composition and spatial location of each scatterer are independent of other scatterers. This may not be the case in biological tissue, especially where scatterers are closely concentrated, limiting the possible locations for each scatterer to exist. Thus, it is not generally true that scatterer positions are uncorrelated. Destrempe and Cloutier [82] proposed that  $\alpha$  does not only describe the average number of scatterers per resolution cell but also their spatial distribution. It was demonstrated using a computational phantom with varying scatterer distributions that estimates for  $1/\alpha$  correlate with an estimated geometric packing factor  $W$  introduced by Twersky [83]. Destrempe and Cloutier [84] later analytically defined the relationship between the  $\alpha$  parameter and the packing factor.

Another complication is introduced when considering different types of scattering which may be present in biological tissue. The derivation of the Rayleigh and successive models relies on the independence of the amplitudes of the phasors that represent each scatter from their phases. For point scatterers, this is true; and for scattering from a compressible sphere, this is generally a sufficient model. However, in the case of cylindrical scattering which may be a more appropriate model for biological components such as muscle, vasculature [61], or bone [85], this assumption is violated. Additionally, speckle models generally use the Born approximation [3], meaning that multiple scattering is not considered.

### B. Measurement of First-Order Speckle Statistics

The first step to characterizing tissue with speckle statistics is acquiring ultrasound data. A PER is selected. Within that region, the size of the resolution cell is assumed to be constant, and the scattering process generating speckle is supposed to be spatially homogeneous. While this is an idealization of the complex scenarios encountered in reality, some recommendations exist to approach this idealization.

**1) Acoustic Field:** The complex summation that results in the speckle interference pattern occurs within the finite-sized resolution cell, defined by the ultrasonic pulse length and beamwidth; for this reason, parameters that affect the acoustic resolution cell can impact speckle statistical estimates. Since characterizing speckle by the Rayleigh distribution relies on the assumption of a large number of scatterers so that the central limit theorem can be applied, it is important to understand approximately what number of scatterers per resolution cell constitutes a large enough number to produce diffuse scattering. Oosterveld et al. [86] showed that the mean amplitude SNR reached the limiting value of 1.91 at densities which corresponds to greater than about eight scatterers per resolution cell for the system analyzed. Tuthill [65] similarly investigated the effects of increasing scatterer density on a 1-D simulated scan and found that SNR achieved a constant value of 1.9 at scatterer densities of 5 per pulse length or greater. Evidently, the commonly cited [24], [25], [34], [52], [87], [88] rule-of-thumb that speckle can be considered fully developed at ten scatterers per resolution cell or greater has a basis in empirical observation.

Tsui and Wang [89] showed that using a nonfocused transducer resulted in high Nakagami values that were insensitive to changes in scatterer density in phantoms, demonstrating that a large resolution cell is undesirable. Tsui and Tsai [90] noted that due to beam divergence with depth, the resolution cell increases in size to encompass more scatterers, causing parameter estimates to approach fully developed speckle. The Nakagami parameter will then approach unity regardless of changing scattering characteristics; this effect is demonstrated in Fig. 6. The authors showed that a multifocus reconstruction approach can mitigate this parameter ambiguity. Yu et al. [91] compared Nakagami parameter values estimated from acquisitions with various beamforming techniques, including synthetic aperture, coherent plane-wave compounding, multifocusing, and single-focusing, to investigate the effects of different resolution cells on speckle

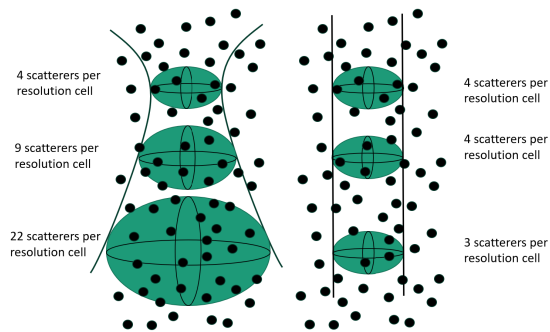


**Fig. 6.** Depth dependence of resolution has significant effects on speckle statistics. The resolution unit, here depicted as an ellipsoid, is defined as the region in space that contributes to a single received signal sample. Strong beam divergence will cause resolution cells to encompass more scatterers as depth increases and speckle statistics will approach the Rayleigh regime. Conversely, if the resolution cell maintains constant size with respect to depth, speckle statistics will be more consistent and maintain sensitivity to microstructural changes. The “scatterer” fields are identical on the left and right of this figure.

estimates. The increasing size of the resolution cell with depth when using single focusing caused a corresponding increase in the Nakagami parameter that was not seen with the other beamforming methods. Thus, Yu et al. recommend using beamforming methods with consistent spatial resolution throughout the image, such as multifocus, synthetic aperture, or plane wave compounding techniques. Mori et al. [92] note a problem in multi-Rayleigh estimation when the ultrasonic beamwidth covers multiple tissue regions, causing ambiguity in the estimation since the resulting signal statistics can be described by a single Rayleigh distribution. Cloutier et al. [93] and Tsui et al. [94] note that envelope statistics of blood and liver tissue, respectively, depend on the carrier frequency due to changing resolution cell size and sensitivity to the presence of coherent scattering.

**2) Independence of Samples:** When estimating parameters of a probability distribution from a dataset, it is assumed that each sample is an independent realization of the underlying statistical process [3]. In the typical ultrasound echo signal, however, the pulse length and beamwidth produce a resolution volume of finite size, so that as the ultrasound beam is scanned across the length of the transducer, overlapping beams will cause adjacent samples to be produced by the same scatterer interaction and thus not independent samples of the statistical process. To appropriately use parameters of probability distributions to describe the statistics of scattering processes, only independent samples should be used. Several authors approximated sample independence by skipping an arbitrary number of samples, but the extent to which sample independence is achieved is unclear in these cases. A more systematic method to approximate sample independence is to only use samples that are at least one correlation length from one another in both axial and lateral directions [25], [26]. However, to our knowledge, the extent to which sample correlation affects speckle statistics analysis has not been systematically studied.

Mori et al. [95] showed analytically and by random number simulation that the number of independent samples in a

signal affects the variance in signal moments, which are used for making parameter estimates. The authors recommend a normalization method that reduces the variance of moment estimates at low sample sizes. Using simulated B-mode images, they also showed that a –6-dB amplitude threshold for designating the size of the point spread function is optimal for determining the number of independent samples in an ROI, agreeing best with the derived relationship between number of independent samples and measured moment variance.

**3) Signal Distortion:** Speckle parameters are estimated using the assumption that the signal intensity reported by the imaging system is linearly related to the degree of backscattered power. However, if for example the signal becomes saturated at high amplitudes as might occur at a high gain setting, this condition is not met, and parameter estimation will be biased due to the uneven tapering at the histogram tail. Hampshire II and Strohbehn [96] noted the bias in Rayleigh, Lognormal, Rician, and Nakagami parameter estimates when signal saturation occurs, and offered Tobit estimators to reduce this bias. However, the limitations of the Tobit estimators make it more desirable to obtain linear data in the first place. Tao et al. [97] address the possibility of system nonlinearity by plotting standard deviation versus mean envelope amplitude for all acquired images; since the resulting plots were linear, they concluded that the data can be appropriately modeled by a unimodal model of scalable distributions. Alternatively, Huang et al. [98] calibrated their receiver system using a known linear relationship between backscattered power and cell concentration at low blood hematocrit.

**4) Log-Compression:** As opposed to raw envelope data which is computed from received RF or IQ echo signals, clinical B-mode images undergo logarithmic compression to enhance weak signals and increase contrast to the viewer. Tuthill [65] showed that logarithmic compression causes a positive shift in the envelope histogram, producing a positive shift in SNR. Dutt and Greenleaf [99] derived a probability density function for the log-compressed envelope from the K distribution. Tsui et al. [100] simulated backscattered signals before and after logarithmic compression to investigate changes in the estimation of Nakagami parameters. While the authors also observed a positive shift in the amplitude histograms after compression, they found that the Nakagami parameter was more sensitive to changing scatterer concentrations when using the histogram of the log-compressed envelope. These Nakagami parameters were not affected by the enforced dynamic range.

It should be noted, however, that the change in amplitude histograms indicates an alteration of the statistical properties of envelope signals, leading to difficulties in the interpretation of parameters. This is also a reason why nonmodel-based approaches could be more flexible than distribution models in practical applications [72], [73], [75].

**5) Spectral Filtration:** Most speckle statistics models and estimation methods assume that received signals contain a single ultrasonic frequency [2], [3], [11], [12], [101], but in practice ultrasound signals have finite frequency bandwidths that vary with depth [2]. Additionally, periodically organized scatterers may produce constructive interference

at some ultrasonic frequencies, and destructive interference at others [7], [8], [12]; therefore, the frequency content of received signals should not be ignored in speckle analysis. Dumane and Shankar [102] demonstrated a way to increase the sensitivity of the Nakagami parameter to scatterer density by using frequency diversity compounding. Their process involves bandpass filtering the received RF at two different frequency ranges, and then summing the corresponding envelopes weighted by the square root of their mean intensities. Tsui et al. [103] note, however, that while sensitivity is improved, the Nakagami parameter is overestimated such that it loses physical meaning. To suppress small signals and improve the sensitivity of the Nakagami parameter to scatterer concentration, they used a noise-assisted empirical mode decomposition to filter backscattered data before computing the Nakagami parameter. This decomposition essentially applies a bank of bandpass filters to the acquired data, using universally applied white noise to establish a baseline for minimum signal strength. The authors demonstrated improved sensitivity compared to raw signals. Bahbah et al. [104] investigated the ability of the Nakagami parameter to provide contrast between tissue-mimicking material and a region containing a high concentration of microbubbles. The contrast was maximized when the received signal was filtered about the second harmonic and the envelope was logarithmically compressed.

**6) Removal of Nonspeckle Signals:** Signals from specular reflectors or those dominated by electronic noise have no real meaning in the context of speckle statistics. Mori et al. [105] investigated the effects of nonspeckle signals from reflective structures such as blood vessels on speckle statistics by analyzing the Kullbeck–Liebler divergence as a function of amplitude. Such nonspeckle signals cause discontinuous spikes in the high-amplitude tails of the echo amplitude histogram, which increase modeling error.

Electronic white noise can cause low contrast-to-noise ratio (CNR) and artifacts in parametric images, especially in anechoic tissue regions [106]. While anechoic regions typically provide high contrast in B-mode images, Tsui et al. observed that demodulated white noise tends to have a Rayleigh-distributed envelope, resulting in the appearance of diffuse scattering according to speckle statistics when they should show no scattering at all. To combat this artifact, Tsui et al. [107] and Tsui [108] proposed a noise-assisted correlation algorithm and later established a requirement for a minimum artificial noise level for the algorithm. In this method, two independent sets of white noise are added to a single RF acquisition, and the correlation between the two noisy data is calculated. Regions of the signal with correlation below the threshold are set to zero since these regions are assumed to be noise-dominated. The authors demonstrated that the algorithm successfully increased the CNR of Nakagami images of anechoic regions. Tsui and Tsai [90] later combined the noise-assisted correlation algorithm with a multifocus approach to demonstrate the overall reduction of Nakagami image artifacts.

**7) Attenuation and Diffraction Compensation:** Since speckle statistics analysis relies on the magnitude of envelope signal

samples, power loss from attenuation and diffraction can also affect parameter estimates. Tuthill [65] noted that simulating RF signals in tissue with attenuation resulted in lower amplitude SNR than without attenuation. Dutt and Greenleaf [11] found that the use of exponential time gain compensation decreased variance in parameter estimation for the homodyned K distribution. Zagzebski et al. [109] investigated the effects of frequency-dependent attenuation on speckle statistics, since the selective attenuation of higher frequencies widens the resolution cell. It was shown that speckle statistics estimates approach diffuse scattering values when greater attenuation is present, and it was suggested that these effects be mitigated by measuring attenuation coefficients and compensating signals accordingly, or by using narrow-band pulses. Nevertheless, in some cases, correction for attenuation may not be necessary, as in the diffuse-to-total signal power ratio presented by Destrempe et al. [20], which was robust to changing attenuation.

Power loss compensation has been applied in a wide variety of ways. For example, Hao et al. [88] demonstrated that increasing attenuation from 0 to 2 dB cm<sup>-1</sup> MHz<sup>-1</sup> causes increasing bias in estimated homodyned K parameters. They proposed an attenuation compensation method in which local attenuation was estimated and then applied inversely to the respective section of RF. Fujii et al. [110] avoided this depth-dependent power loss entirely by choosing estimation regions that were only one RF sample deep. Compared to an estimation region spanning the entire depth of interest, these shallow regions provided lower bias and variance in SNR, skewness, and kurtosis. Huang [111] compensated for diffraction effects using a measured axial beam profile before computing Nakagami parameters. Mamou et al. [112] used a correction factor that was directly applied to homodyned K estimates. The value of the correction factor depended on the center frequency and 6-dB bandwidth of the transducer at a depth of 0 and a depth corresponding to the ROI in a calibration spectrum. Cristea et al. [25] note that attenuation compensation is “essential” for envelope statistics estimates, since high attenuation causes a broadening of the envelope distribution. The authors applied point attenuation compensation to acquired RF spectra and transformed them back to the time domain for parameter estimation. Because combining attenuation with speckle statistics parameters had been shown to improve tissue classification [113], Destrempe et al. [114] forgo direct compensation by including total attenuation coefficient slope in a multiparametric model alongside homodyned K and other quantitative ultrasound parameters.

### C. Parametric Image Considerations

Rather than a single speckle statistic value, a spatial map of estimates, or a parametric map, is often desired. To produce a parametric map, the parameter of interest must be computed over a set of PERs within the acquired data. The size of each PER, sometimes (ambiguously) called the window size, determines not only the spatial resolution of the parametric image but also the stability of the estimates. A large PER will create low-variance, stable estimates but poor resolution, while a small PER size will create a high-resolution image

with high variance. Before creating a parametric image, the PER size must be carefully selected.

Tsui and Chang [115] proposed a method for finding the optimal PER size by comparing the average moment-based Nakagami parameter estimate in square PERs to the average Nakagami parameter estimate for the extent of each scan line, which are assumed to be stable, simulated without acoustic attenuation and beam diffraction. The optimal PER size was chosen such that the estimate values approached equality. Using this method, the ideal PER size was determined to be a square with a side length of three times the pulse length of the incident acoustic wave. It is important to note this result since the three pulse length PER is assumed to be optimal in several later publications within the literature body, even in unrelated systems and experiments.

Fang et al. [116] note, however, that this rule-of-thumb is not universal and should be questioned when using other models like the homodyned K, or when using different estimation methods. Their method for PER size optimization involved maximizing the likelihood that  $\alpha$  and  $k$  parameters of the homodyned K distribution were both real and positive for the same envelope signal. This resulted in a minimum PER side length of seven pulse lengths for their particular system; more than twice the side length previously determined for Nakagami estimation.

Another method for choosing PER size is to calculate some other image quality metric, such as contrast, contrast-to-noise-ratio, or estimate variance, all of which are expected to change as PER size increases. Rosado-Mendez et al. [26] used contrast metrics that showed little change in parameters of the Nakagami and homodyned K distributions beyond 25 correlation lengths; however, PERs were subsampled for uncorrelated amplitude values only, reducing the sample size in each PER. Also of note, homodyned K parameters showed no benefit in contrast over Nakagami parameters in PERs of ten correlation lengths, so higher resolution for lower computation time can be a strength of the Nakagami parameter. Zhou et al. [117], [118] used the change in  $\alpha$  with respect to scatterer concentration to determine an optimal PER size with different estimators.

**1) Sliding Window:** The sliding window method is a simple way to create a parametric image from a collection of PERs [115]. The sliding window method involves: 1) calculating a speckle statistic within a subregion of the ROI, that is, a PER, 2) assigning the statistical parameter to the spatial location at the center of the PER, and 3) shifting the PER spatially and repeating the process. PERs are often allowed to overlap by a predetermined amount to recover some spatial resolution.

In speckle statistics parametric images, it is common to see a variation in the parameter of interest aligned with the boundaries of two regions with different scattering properties. This is not necessarily caused by actual tissue structure, but is an artifact of the way parametric images are constructed: if a PER encompasses two regions with differing underlying statistics, it will not be able to differentiate between them, resulting in an estimate unrepresentative of either region. Larrue and Noble [119] determined that this boundary estimation error as well as those arising from heterogeneity in an ROI, as opposed

to strictly scatterer geometry, may be the factors that drive the ability of the Nakagami parameter to differentiate between tissues. One way the boundary effect can be mitigated is by using smaller window sizes [72], which limits the stability of estimates and the models that are feasible to use. Shankar [58] demonstrated that the gamma mixture and McKay models have better fits according to chi-square values compared to the Nakagami model in PERs encompassing diverse scattering conditions. However, the parameter estimates did not necessarily imply the appropriate scattering conditions (i.e., diffuse scattering in the diffuse scattering target phantom), so the problem of incorrect characterization remains.

**2) Other Windowing Methods:** The sliding window method may leave further smoothing to be desired, especially when imaging homogeneous tissues [120]. The window-modulated compounding method (WMC) involves combining parametric images created using windows (PERs) of different sizes to smooth a Nakagami image, taking advantage of fine resolution and low variance estimates. It has been argued in 2-D [120] and 3-D [121] Nakagami imaging that WMC can improve Nakagami image smoothness without the loss of resolution.

In the case of heterogeneous tissues, WMC may average out important details from small windows. Additionally, computing numerous Nakagami images adds computational complexity. The coarse-to-fine (CTF) method was proposed to address these disadvantages [122]. For this method, an acquired envelope image is designated as layer zero and then downsampled and convolved with a Gaussian blur to produce additional image layers. The topmost layer is used to create a Nakagami image, and this image is used as an initial value for recursive Bowman-estimated Nakagami images on the next layer down. This is repeated until a Nakagami image for the original envelope, the zeroeth layer, is reached. The window size of each layer is constant. It has been shown that using the CTF method provided improved resolution with lower RMSE compared to the sliding window method [122]. Due to the improved image smoothness, boundary artifacts do not appear to be as pronounced in images produced by WMC or CTF as in the simpler sliding window method.

**3) Parametric Image Evaluation:** After the parametric image is formed, an ROI is typically selected to perform statistical analyses between parametric images. For example, contrast metrics, texture analysis [123], [124], and changes in spatially averaged parameters over time or disease state are common. More complex processing, such as contrast weighted summation of parametric maps [125], can also be found in the literature. Tsui et al. [126] suggest: 1) using a relatively small ROI in the same anatomical region of all scans (in their case, in the liver); 2) excluding nonspeckle signals such as vessels; and 3) locating the ROI in the focal zone to reduce the effects of diffraction and attenuation on analysis. As the above discussion of windowing methods suggests, high variance of parameter estimates can create the appearance of heterogeneity that does not exist in underlying tissue; therefore, interpretation of parametric images should always be done within the context of expected estimation errors.

#### IV. DISCUSSION

The wide applications of speckle statistics in tissue characterization have motivated clinical implementation in at least two commercial ultrasound systems [13], [14], with initial applications in steatosis assessment. Interest in these parameters is not limited to the liver, however, as ASQ has been used for applications in the thyroid as well [127]. In addition, there is interest in adding speckle statistics to radiomics feature extraction alongside other ultrasonic measurements like elasticity parameters, backscatter and attenuation coefficients, and texture features. For example, these techniques have been investigated in liver [114], [128], [129], skeletal muscle [130], [131], breast [132], [133], [134], and vasculature [113], [135], [136]. The increasing popularity of these multimodal techniques underscores the necessity of repeatable measurements, as well as an interpretation that accounts for underlying assumptions and the appropriateness of models. Otherwise, improvements in detection capability come at the cost of understanding what these measurements actually mean.

Further clinical translation of speckle statistics parameters necessitates additional research to fill current gaps in knowledge. First, assumptions inherent in speckle statistics such as the presence of weak point scatterers need to be critically examined against the realities of the relevant biological structures. Current speckle statistics models do not account for multiple scattering, finite scatterer size, or specular reflection and may be poor descriptors of tissues where these interactions are prominent. Specialized phantoms and simulations informed by histology may be necessary to quantify departures from the chosen model.

Second, estimation methods require standardization and reduction of error. Numerous potential sources of estimation bias, such as beam divergence, system nonlinearity, and nonspeckle signals cast doubt on reported parameters. Furthermore, choices such as the use of logarithmic compression or whether to compensate for attenuation are a source of confusion and hamper comparison across studies. Rigorous standardization also opens the possibility of system independence, if system effects like diffraction can be corrected.

Third, parameters must be reported in the context of error to be meaningful in diagnostic imaging. Rigorous systematic trials in phantoms, ex vivo tissue, and in vivo tissue are required for a better understanding of expected bias and variance in parameter estimates. Successful clinical translation requires the involvement and education of clinicians to ensure that these parameters are used beneficially and interpreted appropriately. The challenges of interpreting speckle statistics parameters are clear from the variety of models and methods available to the researcher using speckle statistics.

Additional research opportunities lie in expanding the capabilities of speckle statistics to new horizons. Tissues such as the lungs, nerves, and brain have relatively little coverage in the literature. It is possible that speckle statistics can provide untapped information for diagnosis and treatment of disease in these tissues. Also, improvements to the computational efficiency of parameter estimation may facilitate implementation

on portable or point-of-care devices if the estimate variance is sufficiently low.

This review has several limitations that must be considered. Articles found on the Pubmed and Scopus databases were scanned for inclusion by title and abstract, and it is possible that articles were excluded if the relevancy was not clear in these fields. Ideally, the SnowGlobe search should account for any significant articles missed; however, only results with five or more connections to the literature body were included, so it is possible that some relevant articles were neglected. Additionally, blindness to authorship was not feasible in this work.

Speckle statistics offer information about subresolution structures not observable in B-mode ultrasound images. However, while the core paradigm behind image speckle is deceptively simple, numerous complications can be found when considering the realities of clinical imaging. While existing methods have proven useful in tissue characterization, opportunities to address and question simplifications in modeling have great potential. Although differentiating between tissue types and disease states is useful, the utility of speckle statistics could be powerfully extended if they could fundamentally measure tissue properties, allowing not only diagnosis but also understanding and designing interventions for disease.

#### V. CONCLUSION

A systematized review of first-order speckle statistics literature in biomedical ultrasound was performed. A total of 388 relevant articles were discovered using the NIH Pubmed database and Elsevier's Scopus database plus a secondary search of cited works within the literature body. Priority was given to summarizing the models and methods available and to tracking model assumptions. Numerous measurement factors may bias speckle statistics estimates, and careful removal of confounding factors can improve the ability to describe tissue microstructure with speckle statistics. While various authors within this field have proposed solutions to address foundational assumptions in speckle statistics models, relatively few published works have explicitly put these recommendations into practice. Opportunities for expansion of knowledge in speckle statistics lie in addressing discrepancies between simplified models and complex biological realities.

#### ACKNOWLEDGMENT

The authors thank Leslie Christensen of Ebling Library for the Health Sciences at the University of Wisconsin, Madison, for her indispensable help and advisement in performing the search for relevant literature.

#### REFERENCES

- [1] R. F. Wagner, S. W. Smith, J. M. Sandrik, and H. Lopez, "Statistics of speckle in ultrasound B-scans," *IEEE Trans. Sonics Ultrason.*, vol. SU-30, no. 3, pp. 156–163, May 1983.
- [2] R. Cobbold, *Foundations of Biomedical Ultrasound*. New York, NY, USA: Oxford Univ. Press, 2007, pp. 297–298.

- [3] F. Destrempe and G. Cloutier, "Review of envelope statistics models for quantitative ultrasound imaging and tissue characterization," in *Quantitative Ultrasound in Soft Tissues*, J. Mamou and M. L. Oelze, Eds. Dordrecht, The Netherlands: Springer, 2013, ch. 10.
- [4] M. Insana and D. Brown, *Acoustic Scattering Theory Applied to Soft Biological Tissues*. Boca Raton, FL, USA: CRC Press, 1993.
- [5] J. Goodman, "Statistical properties of laser speckle," in *Laser Speckle and Related Phenomena*, J. C. Dainty, Ed. Heidelberg, Germany: Springer, 1975, ch. 9.
- [6] C. B. Burckhardt, "Speckle in ultrasound B-mode scans," *IEEE Trans. Sonics Ultrason.*, vol. SU-25, no. 1, pp. 1–6, Jan. 1978.
- [7] L. Weng, J. M. Reid, P. M. Shankar, K. Soetanto, and X.-M. Lu, "Nonuniform phase distribution in ultrasound speckle analysis. I. Background and experimental demonstration," *IEEE Trans. Ultrason., Ferroelectr., Freq. Control*, vol. 39, no. 3, pp. 352–359, May 1992.
- [8] L. Weng, J. M. Reid, P. M. Shankar, K. Soetanto, and X.-M. Lu, "Nonuniform phase distribution in ultrasound speckle analysis. II. Parametric expression and a frequency sweeping technique to measure mean scatterer spacing," *IEEE Trans. Ultrason., Ferroelectr., Freq. Control*, vol. 39, no. 3, pp. 360–365, May 1992.
- [9] V. M. Narayanan, R. C. Molthen, P. M. Shankar, L. Vergara, and J. M. Reid, "Studies on ultrasonic scattering from quasi-periodic structures," *IEEE Trans. Ultrason., Ferroelectr., Freq. Control*, vol. 44, no. 1, pp. 114–124, Jan. 1997.
- [10] L. Weng, J. M. Reid, P. M. Shankar, and K. Soetanto, "Ultrasound speckle analysis based on the K distribution," *J. Acoust. Soc. Amer.*, vol. 89, no. 6, pp. 2992–2995, Jun. 1991.
- [11] V. Dutt and J. F. Greenleaf, "Ultrasound echo envelope analysis using a homodyned K distribution signal model," *Ultrason. Imag.*, vol. 16, no. 4, pp. 265–287, Oct. 1994.
- [12] P. Mohana Shankar, "A general statistical model for ultrasonic backscattering from tissues," *IEEE Trans. Ultrason., Ferroelectr., Freq. Control*, vol. 47, no. 3, pp. 727–736, May 2000.
- [13] S. K. Jeon, J. M. Lee, and I. Joo, "Clinical feasibility of quantitative ultrasound imaging for suspected hepatic steatosis: Intra- and inter-examiner reliability and correlation with controlled attenuation parameter," *Ultrasound Med. Biol.*, vol. 47, no. 3, pp. 438–445, Mar. 2021.
- [14] J.-Y. Son et al., "Hepatic steatosis: Assessment with acoustic structure quantification of U.S. imaging," *Radiology*, vol. 278, no. 1, pp. 257–264, Jan. 2016.
- [15] M. Grant and A. Booth, "A typology of reviews: An analysis of 14 review types and associated methodologies," *Health Inf. Libraries J.*, vol. 26, pp. 91–108, Jun. 2009.
- [16] S. McWeeny, J. Choe, and E. Norton, "SnowGlobe: An iterative search tool for systematic reviews and meta-analyses," Northwestern Univ., Evanston, IL, USA, Tech. Rep., 2021. [Online]. Available: <https://snowglobe.soc.northwestern.edu/>
- [17] F. Destrempe and G. Cloutier, "A critical review and uniformized representation of statistical distributions modeling the ultrasound echo envelope," *Ultrasound Med. Biol.*, vol. 36, no. 7, pp. 1037–1051, Jul. 2010.
- [18] F. Destrempe, J. Porée, and G. Cloutier, "Estimation method of the homodyned K-distribution based on the mean intensity and two log-moments," *SIAM J. Imag. Sci.*, vol. 6, no. 3, pp. 1499–1530, Jan. 2013.
- [19] Z. Zhou et al., "Parameter estimation of the homodyned K distribution based on an artificial neural network for ultrasound tissue characterization," *Ultrasonics*, vol. 111, Mar. 2021, Art. no. 106308.
- [20] F. Destrempe, E. Franceschini, F. T. H. Yu, and G. Cloutier, "Unifying concepts of statistical and spectral quantitative ultrasound techniques," *IEEE Trans. Med. Imag.*, vol. 35, no. 2, pp. 488–500, Feb. 2016.
- [21] X. Hu et al., "Assessment of homodyned K distribution modeling ultrasonic speckles from scatterers with varying spatial organizations," *J. Healthcare Eng.*, vol. 2017, pp. 1–14, Sep. 2017.
- [22] A. Fernández, A. Ibáñez, M. Parrilla, L. Elvira, Q. Bassat, and J. Jiménez, "Estimation of the concentration of particles in suspension based on envelope statistics of ultrasound backscattering," *Ultrasonics*, vol. 116, Sep. 2021, Art. no. 106501.
- [23] M. Martin-Fernandez, R. Cardenes, and C. Alberola-Lopez, "3D-5 parameter estimation of the homodyned K distribution based on signal to noise ratio," in *Proc. IEEE Ultrason. Symp.*, Oct. 2007, pp. 158–161.
- [24] D. P. Hruska and M. L. Oelze, "Improved parameter estimates based on the homodyned K distribution," *IEEE Trans. Ultrason., Ferroelectr., Freq. Control*, vol. 56, no. 11, pp. 2471–2481, Nov. 2009.
- [25] A. Cristea, N. Collier, E. Franceschini, J. Mamou, C. Cachard, and O. Basset, "Quantitative assessment of media concentration using the homodyned K distribution," *Ultrasonics*, vol. 101, Feb. 2020, Art. no. 105986.
- [26] I. M. Rosado-Mendez, L. C. Drehfal, J. A. Zagzebski, and T. J. Hall, "Analysis of coherent and diffuse scattering using a reference phantom," *IEEE Trans. Ultrason., Ferroelectr., Freq. Control*, vol. 63, no. 9, pp. 1306–1320, Sep. 2016.
- [27] A. Gao, S. Wu, D.-I. Tai, Z. Zhou, and P.-H. Tsui, "Ultrasonic evaluation of liver fibrosis using the homodyned K distribution with an artificial neural network estimator," in *Proc. IEEE Int. Ultrason. Symp. (IUS)*, Sep. 2021, pp. 1–4.
- [28] Y. Liu et al., "An improved parameter estimator of the homodyned K distribution based on the maximum likelihood method for ultrasound tissue characterization," *Ultrason. Imag.*, vol. 44, no. 4, pp. 142–160, Jul. 2022.
- [29] Y. Liu, B. He, Y. Zhang, X. Lang, R. Yao, and L. Pan, "A study on a parameter estimator for the homodyned K distribution based on table search for ultrasound tissue characterization," *Ultrasound Med. Biol.*, vol. 49, no. 4, pp. 970–981, Apr. 2023.
- [30] A. K. Z. Tehrani, G. Cloutier, A. Tang, I. M. Rosado-Mendez, and H. Rivaz, "Homodyned K-distribution parameter estimation in quantitative ultrasound: Autoencoder and Bayesian neural network approaches," *IEEE Trans. Ultrason., Ferroelectr., Freq. Control*, vol. 71, no. 3, pp. 354–365, Mar. 2024.
- [31] J. Cheng and N. C. Beaulieu, "Maximum-likelihood based estimation of the Nakagami  $m$  parameter," *IEEE Commun. Lett.*, vol. 5, no. 3, pp. 101–103, Mar. 2001.
- [32] R. Kolar, R. Jirik, and J. Jan, "Estimator comparison of the Nakagami- $m$  parameter and its application in echocardiography," *Radioengineering*, vol. 13, no. 1, pp. 8–12, 2004.
- [33] D. Wang et al., "Numerical and experimental investigation of impacts of nonlinear scattering encapsulated microbubbles on Nakagami distribution," *Med. Phys.*, vol. 46, no. 12, pp. 5467–5477, Dec. 2019.
- [34] Z. Zhou, A. Gao, Q. Zhang, W. Wu, S. Wu, and P.-H. Tsui, "Ultrasound backscatter envelope statistics parametric imaging for liver fibrosis characterization: A review," *Ultrason. Imag.*, vol. 42, no. 2, pp. 92–109, Mar. 2020.
- [35] T. Y. T. Yamaguchi and H. H. H. Hachiya, "Estimation of the scatterer distribution of the cirrhotic liver using ultrasonic image," *Jpn. J. Appl. Phys.*, vol. 37, no. 5S, pp. 3093–3096, May 1998.
- [36] T. Y. T. Yamaguchi, H. H. H. Hachiya, K. K. K. Kato, H. F. H. Fukuda, and M. E. M. Ebara, "Extraction of quantitative three-dimensional information from ultrasonic volumetric images of cirrhotic liver," *Jpn. J. Appl. Phys.*, vol. 39, no. 5S, pp. 3266–3269, May 2000.
- [37] T. Y. T. Yamaguchi, H. H. H. Hachiya, N. K. N. Kamiyama, K. I. K. Ikeda, and N. M. N. Moriyasu, "Estimation of characteristics of echo envelope using RF echo signal from the liver," *Jpn. J. Appl. Phys.*, vol. 40, no. 5S, pp. 3900–3904, May 2001.
- [38] T. Yamaguchi, K. Hirai, H. Yamada, M. Ebara, and H. Hachiya, "Evaluation of ultrasonic fiber structure extraction technique using autopsy specimens of liver," *Jpn. J. Appl. Phys.*, vol. 44, no. 6S, pp. 4615–4621, Jun. 2005.
- [39] H. Toyoda et al., "B-mode ultrasound with algorithm based on statistical analysis of signals: Evaluation of liver fibrosis in patients with chronic hepatitis C," *Amer. J. Roentgenol.*, vol. 193, no. 4, pp. 1037–1043, Oct. 2009.
- [40] H. Kuroda, "Non-invasive determination of hepatic steatosis by acoustic structure quantification from ultrasound echo amplitude," *World J. Gastroenterol.*, vol. 18, no. 29, p. 3889, 2012.
- [41] J. Keller et al., "Comparison of acoustic structure quantification (ASQ), shearwave elastography and histology in patients with diffuse hepatopathies," *BMC Med. Imag.*, vol. 15, no. 1, Dec. 2015.
- [42] P. M. Shankar, "Ultrasonic tissue characterization using a generalized Nakagami model," *IEEE Trans. Ultrason., Ferroelectr., Freq. Control*, vol. 48, no. 6, pp. 1716–1720, Nov. 2001.
- [43] P. M. Shankar, "A compound scattering pdf for the ultrasonic echo envelope and its relationship to K and Nakagami distributions," *IEEE Trans. Ultrason., Ferroelectr., Freq. Control*, vol. 50, no. 3, pp. 339–343, Mar. 2003.
- [44] R. Agrawal and Karmeshu, "Study of ultrasonic echo envelope based on Nakagami-inverse Gaussian distribution," *Ultrasound Med. Biol.*, vol. 32, no. 3, pp. 371–376, Mar. 2006.

- [45] R. Agrawal and Karmeshu, "Ultrasonic backscattering in tissue: Characterization through Nakagami-generalized inverse Gaussian distribution," *Comput. Biol. Med.*, vol. 37, no. 2, pp. 166–172, Feb. 2007.
- [46] S. Nadarajah, "Statistical distributions of potential interest in ultrasound speckle analysis," *Phys. Med. Biol.*, vol. 52, no. 10, pp. N213–N227, May 2007.
- [47] Y. Igarashi, H. Ezuka, T. Yamaguchi, and H. Hachiya, "Quantitative estimation method for liver fibrosis based on combination of Rayleigh distributions," *Jpn. J. Appl. Phys.*, vol. 49, no. 7S, Jul. 2010, Art. no. 07HF06.
- [48] T. Higuchi, S. Hirata, T. Yamaguchi, and H. Hachiya, "Quantitative evaluation of liver fibrosis using multi-Rayleigh model with hypoechoic component," *Jpn. J. Appl. Phys.*, vol. 52, no. 7S, Jul. 2013, Art. no. 07HF19.
- [49] J. C. Seabra, F. Ciompi, O. Pujol, J. Mauri, P. Radeva, and J. Sanches, "Rayleigh mixture model for plaque characterization in intravascular ultrasound," *IEEE Trans. Biomed. Eng.*, vol. 58, no. 5, pp. 1314–1324, May 2011.
- [50] S. Mori, S. Hirata, T. Yamaguchi, and H. Hachiya, "Quantitative evaluation method for liver fibrosis based on multi-Rayleigh model with estimation of number of tissue components in ultrasound B-mode image," *Jpn. J. Appl. Phys.*, vol. 57, no. 7S1, Jul. 2018, Art. no. 07LF17.
- [51] C. Zhang, S. Mori, S. Hirata, and H. Hachiya, "Examination of optimal moments as input parameters for evaluation of liver fibrosis based on multi-Rayleigh model," *Jpn. J. Appl. Phys.*, vol. 57, no. 7S1, Jul. 2018, Art. no. 07LF27.
- [52] K. Tamura, K. Yoshida, H. Maruyama, H. Hachiya, and T. Yamaguchi, "Proposal of compound amplitude envelope statistical analysis model considering low scatterer concentration," *Jpn. J. Appl. Phys.*, vol. 57, no. 7S1, Jul. 2018, Art. no. 07LD19.
- [53] P. M. Shankar, F. Forsberg, and L. Lown, "Statistical modeling of atherosclerotic plaque in carotid B mode images—A feasibility study," *Ultrasound Med. Biol.*, vol. 29, no. 9, pp. 1305–1309, Sep. 2003.
- [54] F. Destrempes, J. Meunier, M.-F. Giroux, G. Soulez, and G. Cloutier, "Segmentation in ultrasonic B-mode images of healthy carotid arteries using mixtures of Nakagami distributions and stochastic optimization," *IEEE Trans. Med. Imag.*, vol. 28, no. 2, pp. 215–229, Feb. 2009.
- [55] G. Vegas-Sánchez-Ferrero et al., "Gamma mixture classifier for plaque detection in intravascular ultrasonic images," *IEEE Trans. Ultrason., Ferroelectr., Freq. Control*, vol. 61, no. 1, pp. 44–61, Jan. 2014.
- [56] X. Huang et al., "Identification of ultrasonic echolucent carotid plaques using discrete Fréchet distance between bimodal gamma distributions," *IEEE Trans. Biomed. Eng.*, vol. 65, no. 5, pp. 949–955, May 2018.
- [57] S. Sikdar et al., "Quantification of muscle tissue properties by modeling the statistics of ultrasound image intensities using a mixture of gamma distributions in children with and without cerebral palsy," *J. Ultrasound Med.*, vol. 37, no. 9, pp. 2157–2169, Sep. 2018.
- [58] P. M. Shankar, "Statistics of boundaries in ultrasonic B-scan images," *Ultrasound Med. Biol.*, vol. 41, no. 1, pp. 268–280, Jan. 2015.
- [59] G. Vegas-Sánchez-Ferrero, S. Aja-Fernandez, C. Palencia, and M. Martín-Fernández, "A generalized gamma mixture model for ultrasonic tissue characterization," *Comput. Math. Methods Med.*, vol. 2012, pp. 1–25, Aug. 2012.
- [60] P. M. Shankar, "A statistical model for the ultrasonic backscattered echo from tissue containing microcalcifications," *IEEE Trans. Ultrason., Ferroelectr., Freq. Control*, vol. 60, no. 5, pp. 932–942, May 2013.
- [61] K. J. Parker, "The first order statistics of backscatter from the fractal branching vasculature," *J. Acoust. Soc. Amer.*, vol. 146, no. 5, pp. 3318–3326, Nov. 2019.
- [62] K. J. Parker and S. S. Poul, "Burr, lomax, Pareto, and logistic distributions from ultrasound speckle," *Ultrason. Imag.*, vol. 42, nos. 4–5, pp. 203–212, Jul. 2020.
- [63] M. R. Lowerison, J. J. Tse, M. N. Hague, A. F. Chambers, D. W. Holdsworth, and J. C. Lacefield, "Compound speckle model detects anti-angiogenic tumor response in preclinical nonlinear contrast-enhanced ultrasonography," *Med. Phys.*, vol. 44, no. 1, pp. 99–111, Jan. 2017.
- [64] A. Vieli, "An improved stochastic approach to RF amplitude analysis in ultrasonic cardiac tissue characterization," *Ultrason. Imag.*, vol. 6, no. 2, pp. 139–151, Apr. 1984.
- [65] T. Tuthill, "Deviations from Rayleigh statistics in ultrasonic speckle," *Ultrason. Imag.*, vol. 9, no. 1, pp. 58–59, Jan. 1987.
- [66] V. Dutt, "Speckle analysis using signal to noise ratios based on fractional order moments," *Ultrason. Imag.*, vol. 17, no. 4, pp. 251–268, Oct. 1995.
- [67] R. Kuc, "Ultrasonic tissue characterization using kurtosis," *IEEE Trans. Ultrason., Ferroelectr., Freq. Control*, vol. UFFC-33, no. 3, pp. 273–279, May 1986.
- [68] H.-Y. Ma, Z. Zhou, S. Wu, Y.-L. Wan, and P.-H. Tsui, "A computer-aided diagnosis scheme for detection of fatty liver in vivo based on ultrasound kurtosis imaging," *J. Med. Syst.*, vol. 40, no. 1, p. 33, Jan. 2016.
- [69] M. S. Hughes, "Analysis of digitized waveforms using Shannon entropy," *J. Acoust. Soc. Amer.*, vol. 93, no. 2, pp. 892–906, Feb. 1993.
- [70] Y. Zimmer, S. Akselrod, and R. Tepper, "The distribution of the local entropy in ultrasound images," *Ultrasound Med. Biol.*, vol. 22, no. 4, pp. 431–439, Jan. 1996.
- [71] P. Tsui, "Information entropy and its applications," in *Quantitative Ultrasound in Soft Tissues*, J. Mamou and M. L. Oelze, Eds., 2nd ed. Cham, Switzerland: Springer, 2023, ch. 8.
- [72] P.-H. Tsui et al., "Small-window parametric imaging based on information entropy for ultrasound tissue characterization," *Sci. Rep.*, vol. 7, no. 1, Jan. 2017, Art. no. 41004.
- [73] Z. Zhou et al., "Hepatic steatosis assessment with ultrasound small-window entropy imaging," *Ultrasound Med. Biol.*, vol. 44, no. 7, pp. 1327–1340, Jul. 2018.
- [74] Y.-L. Lee et al., "Characterization of limb lymphedema using the statistical analysis of ultrasound backscattering," *Quant. Imag. Med. Surg.*, vol. 10, no. 1, pp. 48–56, Jan. 2020.
- [75] R. Smolikova, M. P. Wachowiak, and J. M. Zurada, "An information-theoretic approach to estimating ultrasound backscatter characteristics," *Comput. Biol. Med.*, vol. 34, no. 4, pp. 355–370, Jun. 2004.
- [76] H.-J. Chan et al., "Ultrasound sample entropy imaging: A new approach for evaluating hepatic steatosis and fibrosis," *IEEE J. Transl. Eng. Health Med.*, vol. 9, pp. 1–12, 2021.
- [77] A. Sorrento, A. Poliziani, A. Cafarelli, G. Valenza, and L. Ricotti, "A novel quantitative and reference-free ultrasound analysis to discriminate different concentrations of bone mineral content," *Sci. Rep.*, vol. 11, no. 1, Jan. 2021, Art. no. 301.
- [78] X. Li et al., "Ultrasound entropy imaging for detection and monitoring of thermal lesion during microwave ablation of liver," *IEEE J. Biomed. Health Inform.*, vol. 26, no. 8, pp. 4056–4066, Aug. 2022.
- [79] R. Gao, P.-H. Tsui, S. Wu, D.-I. Tai, G. Bin, and Z. Zhou, "Ultrasound entropy imaging based on the kernel density estimation: A new approach to hepatic steatosis characterization," *Diagnostics*, vol. 13, no. 24, p. 3646, Dec. 2023.
- [80] S. Li, P.-H. Tsui, W. Wu, S. Wu, and Z. Zhou, "Ultrasound K-nearest neighbor entropy imaging: Theory, algorithm, and applications," *Ultrasound*, vol. 138, Mar. 2024, Art. no. 107256.
- [81] P. M. Shankar et al., "Studies on the use of non-Rayleigh statistics for ultrasonic tissue characterization," *Ultrasound Med. Biol.*, vol. 22, no. 7, pp. 873–882, Jan. 1996.
- [82] F. Destrempes and G. Cloutier, "Interpretation based on stochastic geometry of homodyned-K distribution scatterer clustering parameter for quantitative ultrasound imaging," in *Proc. IEEE Int. Ultrason. Symp. (IUS)*, Sep. 2020, pp. 1–4.
- [83] V. Twersky, "Low-frequency scattering by correlated distributions of randomly oriented particles," *J. Acoust. Soc. Amer.*, vol. 81, no. 5, pp. 1609–1618, May 1987.
- [84] F. Destrempes and G. Cloutier, "Statistical modeling of ultrasound signals related to the packing factor of wave scattering phenomena for structural characterization," *J. Acoust. Soc. Amer.*, vol. 150, no. 5, pp. 3544–3556, Nov. 2021.
- [85] J. Litniewski, L. Cieslik, J. Wojcik, and A. Nowicki, "Statistics of the envelope of ultrasonic backscatter from human trabecular bone," *J. Acoust. Soc. Amer.*, vol. 130, no. 4, pp. 2224–2232, Oct. 2011.
- [86] B. Oosterveld, "Texture of B-mode echograms: 3-D simulations and experiments of the effects of diffraction and scatterer density," *Ultrason. Imag.*, vol. 7, no. 2, pp. 142–160, Apr. 1985.
- [87] R. M. Cramblitt and K. J. Parker, "Generation of non-Rayleigh speckle distributions using marked regularity models," *IEEE Trans. Ultrason., Ferroelectr., Freq. Control*, vol. 46, no. 4, pp. 867–874, Jul. 1999.
- [88] X. Hao, C. J. Bruce, C. Pislaru, and J. F. Greenleaf, "Characterization of reperfused infarcted myocardium from high-frequency intracardiac ultrasound imaging using homodyned K distribution," *IEEE Trans. Ultrason., Ferroelectr., Freq. Control*, vol. 49, no. 11, pp. 1530–1542, Nov. 2002.

- [89] P.-H. Tsui and S.-H. Wang, "The effect of transducer characteristics on the estimation of Nakagami parameter as a function of scatterer concentration," *Ultrasound Med. Biol.*, vol. 30, no. 10, pp. 1345–1353, Oct. 2004.
- [90] P.-H. Tsui and Y.-W. Tsai, "Artifact reduction of ultrasound Nakagami imaging by combining multifocus image reconstruction and the noise-assisted correlation algorithm," *Ultron. Imag.*, vol. 37, no. 1, pp. 53–69, Jan. 2015.
- [91] X. Yu, Y. Guo, S.-M. Huang, M.-L. Li, and W.-N. Lee, "Beamforming effects on generalized Nakagami imaging," *Phys. Med. Biol.*, vol. 60, no. 19, pp. 7513–7531, Oct. 2015.
- [92] S. Mori, S. Hirata, and H. Hachiya, "Effect of beam width on quantitative estimation of liver fibrosis using ultrasonic images," *Jpn. J. Appl. Phys.*, vol. 53, no. 7S, Jul. 2014, Art. no. 07KF23.
- [93] G. Cloutier, M. Daronat, D. Savéry, D. Garcia, L.-G. Durand, and F. S. Foster, "Non-Gaussian statistics and temporal variations of the ultrasound signal backscattered by blood at frequencies between 10 and 58 MHz," *J. Acoust. Soc. Amer.*, vol. 116, no. 1, pp. 566–577, Jul. 2004.
- [94] P.-H. Tsui, Z. Zhou, Y.-H. Lin, C.-M. Hung, S.-J. Chung, and Y.-L. Wan, "Effect of ultrasound frequency on the Nakagami statistics of human liver tissues," *PLoS ONE*, vol. 12, no. 8, Aug. 2017, Art. no. e0181789.
- [95] S. Mori, M. Arakawa, H. Kanai, and H. Hachiya, "Quantification of limitations in statistical analysis of ultrasound echo envelope amplitudes," *Jpn. J. Appl. Phys.*, vol. 62, no. SJ, Jul. 2023, Art. no. SJ1045.
- [96] J. B. Hampshire and J. W. Strohbehn, "Tobit maximum-likelihood estimation for stochastic time series affected by receiver saturation," *IEEE Trans. Inf. Theory*, vol. 38, no. 2, pp. 457–469, Mar. 1992.
- [97] Z. Tao, H. D. Tagare, and J. D. Beaty, "Evaluation of four probability distribution models for speckle in clinical cardiac ultrasound images," *IEEE Trans. Med. Imag.*, vol. 25, no. 11, pp. 1483–1491, Nov. 2006.
- [98] C.-C. Huang, P.-H. Tsui, and S.-H. Wang, "Detection of coagulating blood under steady flow by statistical analysis of backscattered signals," *IEEE Trans. Ultrason., Ferroelectr., Freq. Control*, vol. 54, no. 2, pp. 435–442, Feb. 2007.
- [99] V. Dutt and J. F. Greenleaf, "Statistics of the log-compressed echo envelope," *J. Acoust. Soc. Amer.*, vol. 99, no. 6, pp. 3817–3825, Jun. 1996.
- [100] P.-H. Tsui, S.-H. Wang, and C.-C. Huang, "The effect of logarithmic compression on estimation of the Nakagami parameter for ultrasonic tissue characterization: A simulation study," *Phys. Med. Biol.*, vol. 50, no. 14, pp. 3235–3244, Jul. 2005.
- [101] M. Ohta, S. Miyata, and N. Nakasako, "Generalization of Rician distribution for speckle pattern in ultrasound image processing and random flights problem in Shannon's signal space," *J. Acoust. Soc. Jpn. E*, vol. 13, no. 2, pp. 101–113, 1992.
- [102] V. A. Dumane and P. M. Shankar, "Use of frequency diversity and Nakagami statistics in ultrasonic tissue characterization," *IEEE Trans. Ultrason., Ferroelectr., Freq. Control*, vol. 48, no. 4, pp. 1139–1146, Jul. 2001.
- [103] P.-H. Tsui, Y.-L. Wan, C.-C. Huang, and M.-C. Wang, "Effect of adaptive threshold filtering on ultrasonic Nakagami parameter to detect variation in scatterer concentration," *Ultron. Imag.*, vol. 32, no. 4, pp. 229–242, Oct. 2010.
- [104] N. Bahbah, A. Novell, A. Bouakaz, and H. Djelouah, "Linear and non-linear characterization of microbubbles and tissue using the Nakagami statistical model," *Ultrasonics*, vol. 76, pp. 200–207, Apr. 2017.
- [105] S. Mori, S. Hirata, T. Yamaguchi, and H. Hachiya, "Probability image of tissue characteristics for liver fibrosis using multi-Rayleigh model with removal of nonspeckle signals," *Jpn. J. Appl. Phys.*, vol. 54, no. 7S1, Jul. 2015, Art. no. 07HF20.
- [106] P.-H. Tsui, C.-K. Yeh, C.-C. Chang, and W.-S. Chen, "Performance evaluation of ultrasonic Nakagami image in tissue characterization," *Ultron. Imag.*, vol. 30, no. 2, pp. 78–94, Apr. 2008.
- [107] P.-H. Tsui, C.-K. Yeh, and C.-C. Huang, "Noise-assisted correlation algorithm for suppressing noise-induced artifacts in ultrasonic Nakagami images," *IEEE Trans. Inf. Technol. Biomed.*, vol. 16, no. 3, pp. 314–322, May 2012.
- [108] P.-H. Tsui, "Minimum requirement of artificial noise level for using noise-assisted correlation algorithm to suppress artifacts in ultrasonic Nakagami images," *Ultron. Imag.*, vol. 34, no. 2, pp. 110–124, Apr. 2012.
- [109] J. A. Zagzebski, J.-F. Chen, F. Dong, and T. Wilson, "Intervening attenuation affects first-order statistical properties of ultrasound echo signals," *IEEE Trans. Ultrason., Ferroelectr., Freq. Control*, vol. 46, no. 1, pp. 35–40, Jan. 1999.
- [110] Y. Fujii et al., "Clinical application of a new method that segments the region of interest into multiple layers for RF amplitude histogram analysis in the cirrhotic liver," *J. Med. Ultrason.*, vol. 31, no. 2, pp. 91–98, Jun. 2004.
- [111] C.-C. Huang, "Detecting spatial variations of erythrocytes by ultrasound backscattering statistical parameters under pulsatile flow," *IEEE Trans. Biomed. Eng.*, vol. 58, no. 5, pp. 1163–1171, May 2011.
- [112] J. Mamou et al., "Three-dimensional high-frequency backscatter and envelope quantification of cancerous human lymph nodes," *Ultrasound Med. Biol.*, vol. 37, no. 3, pp. 345–357, Mar. 2011.
- [113] D. Sheet et al., "Joint learning of ultrasonic backscattering statistical physics and signal confidence primal for characterizing atherosclerotic plaques using intravascular ultrasound," *Med. Image Anal.*, vol. 18, no. 1, pp. 103–117, Jan. 2014.
- [114] F. Destremps et al., "Quantitative ultrasound, elastography, and machine learning for assessment of steatosis, inflammation, and fibrosis in chronic liver disease," *PLoS ONE*, vol. 17, no. 1, Jan. 2022, Art. no. e0262291.
- [115] P. Tsui and C. Chang, "Imaging local scatterer concentrations by the Nakagami statistical model," *Ultrasound Med. Biol.*, vol. 33, no. 4, pp. 608–619, 2007.
- [116] J. Fang, Z. Zhou, N.-F. Chang, Y.-L. Wan, and P.-H. Tsui, "Ultrasound parametric imaging of hepatic steatosis using the homodyned-K distribution: An animal study," *Ultrasonics*, vol. 87, pp. 91–102, Jul. 2018.
- [117] Z. Zhou et al., "Hepatic steatosis assessment using ultrasound homodyned-K parametric imaging: The effects of estimators," *Quant. Imag. Med. Surg.*, vol. 9, no. 12, pp. 1932–1947, Dec. 2019.
- [118] Z. Zhou et al., "Value of homodyned K distribution in ultrasound parametric imaging of hepatic steatosis: An animal study," *Ultrasonics*, vol. 101, Feb. 2020, Art. no. 106001.
- [119] A. Larrue and J. A. Noble, "Modeling of errors in Nakagami imaging: Illustration on breast mass characterization," *Ultrasound Med. Biol.*, vol. 40, no. 5, pp. 917–930, May 2014.
- [120] P.-H. Tsui, H.-Y. Ma, Z. Zhou, M.-C. Ho, and Y.-H. Lee, "Window-modulated compounding Nakagami imaging for ultrasound tissue characterization," *Ultrasonics*, vol. 54, no. 6, pp. 1448–1459, Aug. 2014.
- [121] Z. Zhou, S. Wu, M.-Y. Lin, J. Fang, H.-L. Liu, and P.-H. Tsui, "Three-dimensional visualization of ultrasound backscatter statistics by window-modulated compounding Nakagami imaging," *Ultron. Imag.*, vol. 40, no. 3, pp. 171–189, May 2018.
- [122] M. Han, J. Wan, Y. Zhao, X. Zhou, and M. Wan, "Nakagami-m parametric imaging for atherosclerotic plaque characterization using the coarse-to-fine method," *Ultrasound Med. Biol.*, vol. 43, no. 6, pp. 1275–1289, Jun. 2017.
- [123] O. S. Al-Kadi, D. Y. F. Chung, C. C. Coussios, and J. A. Noble, "Heterogeneous tissue characterization using ultrasound: A comparison of fractal analysis backscatter models on liver tumors," *Ultrasound Med. Biol.*, vol. 42, no. 7, pp. 1612–1626, Jul. 2016.
- [124] S. Muhtadi, R. R. Razzaque, A. Chowdhury, B. S. Garra, and S. K. Alam, "Texture quantified from ultrasound Nakagami parametric images is diagnostically relevant for breast tumor characterization," *J. Med. Imag.*, vol. 10, no. S2, Jun. 2023, Art. no. S22410.
- [125] S. Li, Z. Zhou, S. Wu, and W. Wu, "Ultrasound homodyned-K contrast-weighted summation parametric imaging based on H-scan for detecting microwave ablation zones," *Ultron. Imag.*, vol. 45, no. 3, pp. 119–135, May 2023.
- [126] P.-H. Tsui, Y.-L. Wan, D.-I. Tai, and Y.-C. Shu, "Effects of estimators on ultrasound Nakagami imaging in visualizing the change in the backscattered statistics from a Rayleigh distribution to a pre-Rayleigh distribution," *Ultrasound Med. Biol.*, vol. 41, no. 8, pp. 2240–2251, Aug. 2015.
- [127] S. J. Rhee, H. S. Hong, C.-H. Kim, E. H. Lee, J. G. Cha, and S. H. Jeong, "Using acoustic structure quantification during B-mode sonography for evaluation of Hashimoto thyroiditis," *J. Ultrasound Med.*, vol. 34, no. 12, pp. 2237–2243, Dec. 2015.
- [128] A. Han et al., "Assessment of hepatic steatosis in nonalcoholic fatty liver disease by using quantitative U.S." *Radiology*, vol. 295, no. 1, pp. 106–113, Apr. 2020.
- [129] Z. Zhou, Z. Zhang, A. Gao, D.-I. Tai, S. Wu, and P.-H. Tsui, "Liver fibrosis assessment using radiomics of ultrasound homodyned-K imaging based on the artificial neural network estimator," *Ultron. Imag.*, vol. 44, nos. 5–6, pp. 229–241, Nov. 2022.
- [130] D. Yan, Q. Li, C.-W. Lin, J.-Y. Shieh, W.-C. Weng, and P.-H. Tsui, "Hybrid QUS radiomics: A multimodal-integrated quantitative ultrasound radiomics for assessing ambulatory function in Duchenne muscular dystrophy," *IEEE J. Biomed. Health Informat.*, vol. 28, no. 2, pp. 835–845, Feb. 2024.

- [131] N. J. Bureau et al., "Diagnostic accuracy of echo envelope statistical modeling compared to B-mode and power Doppler ultrasound imaging in patients with clinically diagnosed lateral epicondylitis of the elbow," *J. Ultrasound Med.*, vol. 38, no. 10, pp. 2631–2641, Oct. 2019.
- [132] Y. Liao et al., "Classification of scattering media within benign and malignant breast tumors based on ultrasound texture-feature-based and Nakagami-parameter images," *Med. Phys.*, vol. 38, no. 4, pp. 2198–2207, Apr. 2011.
- [133] S.-M. Hsu, W.-H. Kuo, F.-C. Kuo, and Y.-Y. Liao, "Breast tumor classification using different features of quantitative ultrasound parametric images," *Int. J. Comput. Assist. Radiol. Surg.*, vol. 14, no. 4, pp. 623–633, Apr. 2019.
- [134] Z. Klimonda, P. Karwat, K. Dobruch-Sobczak, H. Piotrkowska-Wróblewska, and J. Litniewski, "Breast-lesions characterization using quantitative ultrasound features of peritumoral tissue," *Sci. Rep.*, vol. 9, no. 1, p. 7963, May 2019.
- [135] G. Bosio, N. Zenati, F. Destrempe, B. Chayer, G. Pernod, and G. Cloutier, "Shear wave elastography and quantitative ultrasound as biomarkers to characterize deep vein thrombosis *in vivo*," *J. Ultrasound Med.*, vol. 41, no. 7, pp. 1807–1816, Jul. 2022.
- [136] C. Hoerig, K. Wallace, M. Wu, and J. Mamou, "Classification of metastatic lymph nodes *in vivo* using quantitative ultrasound at clinical frequencies," *Ultrasound Med. Biol.*, vol. 49, no. 3, pp. 787–801, Mar. 2023.



**Alexandra M. Christensen** was born in Knoxville, TN, USA, in 1997. She received the B.S. degree in physics from Brigham Young University, Provo, UT, USA, in 2020, and the M.S. degree in medical physics from the University of Wisconsin–Madison, Madison, WI, USA, in 2023.

From 2018 to 2020, she was a Research Assistant with the Department of Radiation Oncology, University of California at San Francisco, San Francisco, CA, USA. Since 2020, she has been a Graduate Researcher with the Quantitative Ultrasound Laboratory, University of Wisconsin–Madison. Her research interests include refining quantitative ultrasound techniques to improve the characterization of cervix tissue throughout pregnancy, especially with the use of speckle statistics.



**Ivan M. Rosado-Mendez** (Member, IEEE) was born in Mérida, Mexico. He received the B.S. degree in engineering physics from the Tecnológico de Monterrey, Monterrey, Mexico, in 2006, the M.S. degree in medical physics from the National Autonomous University of Mexico, Mexico City, Mexico, in 2009, and the Ph.D. degree in medical physics from the University of Wisconsin–Madison, Madison, WI, USA, in 2014.

He is currently an Assistant Professor with the Department of Medical Physics and Radiology, University of Wisconsin–Madison. His research interests include the quantification of coherent and incoherent ultrasonic scattering for tissue characterization and the analysis of tissue viscoelasticity using shear wave elastography.



**Timothy J. Hall** (Life Member, IEEE) received the B.A. degree in physics from the University of Michigan–Flint, Flint, MI, USA, in 1983, and the M.S. and Ph.D. degrees in medical physics from the University of Wisconsin–Madison, Madison, WI, USA, in 1985 and 1988, respectively.

From 1988 to 2002, he was with the Radiology Department, The University of Kansas Medical Center, Kansas City, KS, USA, where he worked on the measurements of acoustic scattering in tissues, metrics of observer performance in ultrasound imaging, and developed elasticity imaging methods and phantoms for elasticity imaging. In 2003, he returned to the University of Wisconsin–Madison, where he is currently a Professor in the Medical Physics Department. From 2012 to 2023, he served in leadership roles in the Quantitative Imaging Biomarkers Alliance serving as the Chair for the organization from 2021 to 2023. His research interests continue to center on developing new image formation strategies based on acoustic wave propagation and tissue viscoelasticity, the development of methods for system performance evaluation, and quantitative biomarker development.